

A new jamming scenario: from marginal jamming to deep jamming

Cang Zhao, Kaiwen Tian, and Ning Xu*

Department of Physics, University of Science and Technology of China, Hefei 230026, P. R. China

(Dated: June 26, 2019)

We study properties of jammed packings of frictionless spheres over a wide range of volume fractions. There exists a crossover volume fraction which separates deeply jammed solids from marginally jammed solids. In deeply jammed solids, all the scalings presented in marginally jammed solids are replaced with remarkably different ones independent on the inter-particle potentials studied here. Correspondingly, there are structural changes in the pair distribution function associated with the crossover. The normal modes of vibration of deeply jammed solids also exhibit some anomalies, e.g. strengthened quasi-localization and absence of Debye-like density of states at low frequencies. Deeply jammed systems may thus be cataloged to a new class of amorphous solids.

PACS numbers: 63.50.Lm, 61.43.-j, 63.20.Pw

Colloidal suspensions and granular materials jam into amorphous solids when they are so compact that there is no room for constituent particles to move freely. As a simplified model to study the formation of this rigidity, a packing of frictionless soft spheres undergoes the jamming transition labeled “J” at a critical volume fraction ϕ_c [1–5]. Point J exhibits unusual criticality in the presence of diverging length scales [6–13], vanishing length scales in the pair distribution function $g(r)$ [14–16], and critical scalings of a variety of quantities which depend on inter-particle potential [5, 7, 8, 13, 17]. The normal modes of vibration in marginally jammed solids near Point J also possess some anomalous properties. For instance, low-frequency modes are quasi-localized, anharmonic, and poor in energy conduction [13, 18, 19], contrary to plane-waves in normal solids. Some special vibrational features have been recently observed in experiments as well [20–23].

Although great efforts have been made to understand the anomalous properties of marginally jammed solids, it has not yet been questioned whether these properties would persist when the volume fraction keeps increasing away from Point J. If not, beyond what volume fraction will our present knowledge about jamming fail to describe the solids in the new regime which may be defined as deeply jammed solids? Are there any special properties of deeply jammed solids? We may intuitively expect that jammed solids at high volume fractions would be more spatially homogeneous, so that they might be more “normal” and “mean-field”.

In this letter, we extend the study of jammed solids to high volume fractions in order to address the above questions. The critical scalings well-known in marginally jammed solids no longer hold in dense systems. Surprisingly, the scalings, structure, and vibrational properties of jammed solids undergo significant changes at approximately the same crossover volume fraction ϕ_d . The existent knowledge of jammed solids is thus limited to marginal jamming at $\phi_c < \phi < \phi_d$. Moreover, properties of normal modes of vibration in deeply jammed solids at $\phi > \phi_d$ are beyond our understanding of both normal solids like crystals and marginally jammed solids.

The three-dimensional systems studied here consist of a 50 : 50 binary mixture of $N = 1000$ frictionless spheres interacting via a spring-like repulsion: $V(r_{ij}) = \epsilon(1 - r_{ij}/\sigma_{ij})^\alpha/\alpha$ when the inter-particle separation of particles i and j , r_{ij} is less than the sum of their radii, $\sigma_{ij} = (\sigma_i + \sigma_j)/2$, and 0 otherwise. Periodic boundary conditions are applied in all directions. The diameter ratio of the two species is 1.4 to avoid crystallization. This model has been widely adopted in the study of jamming and the glass transition. We apply L-BFGS energy minimization method [24] to obtain local energy minima and tune the volume fraction successively to obtain jammed packings of spheres at desired pressure p . At each pressure, we generate 1000 jammed states and take averages over them. We set the small particle diameter σ , particle mass m , and ϵ to be one. The frequency is thus in the units of $\sqrt{\epsilon/m\sigma^2}$.

Figure 1 shows the potential energy per particle, V , bulk modulus, B , shear modulus, G , and coordination number, z versus the volume fraction ϕ for both harmonic ($\alpha = 2$) and Hertzian ($\alpha = 5/2$) systems [25]. In marginally jammed solids ($\phi < \phi_d$), our data are fitted well with the following well-known scalings [5]:

$$\begin{aligned} V &\sim (\phi - \phi_c)^\alpha, & B &\sim \phi(\phi - \phi_c)^{\alpha-2}, \\ G &\sim (\phi - \phi_c)^{\alpha-3/2}, & z - z_c &\sim (\phi - \phi_c)^{1/2}. \end{aligned} \quad (1)$$

where $\phi_c \approx 0.6446$ for $\alpha = 2$ and 0.6443 for $\alpha = 5/2$, and $z_c = 2d$ is the isostatic value at Point J with d the dimension of space. Most of these scalings depend on the inter-particle potential, which is one of the particularities of the jamming transition at Point J. Note that the fits to the bulk modulus using Eq. (1) slightly deviate from the data, as shown in Fig. 1(b). It is because that the bulk modulus in Eq. (1) is derived from the widely accepted relation $p \sim (\phi - \phi_c)^{\alpha-1}$, but the actual exponent is slightly larger than $\alpha - 1$ [26].

The scalings described in Eq. (1) break down in the vicinity of a crossover volume fraction $\phi_d \approx 1.20 \pm 0.20$ ($\phi_d - \phi_c \approx 0.55 \pm 0.20$) which is approximately the same for both potentials studied here. When $\phi > \phi_d$, all the scalings in Eq. (1) turn into new power laws with inter-

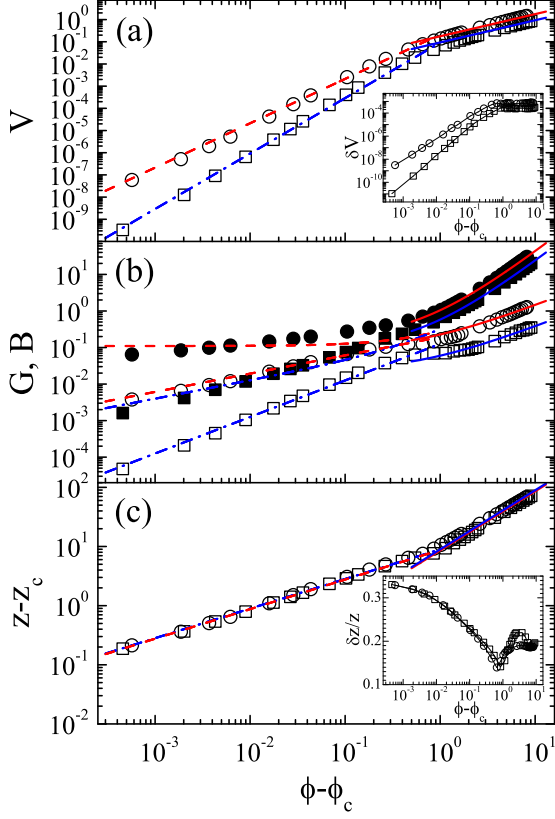


FIG. 1: (color online) (a) Potential energy per particle V , (b) shear modulus G (empty symbols), bulk modulus B (solid symbols), and (c) excess coordination number above isotacticity $z - z_c$ versus $\phi - \phi_c$ of jammed systems with harmonic ($\alpha = 2$, circles) and Hertzian ($\alpha = 5/2$, squares) interactions. The red dashed (harmonic) and blue dot-dashed (Hertzian) lines are fits for marginally jammed solids according to Eq. (1), while the solid curves are fits for deeply jammed solids according to Eq. (2). The insets to (a) and (c) show the half height width of the potential energy distribution at fixed pressure, δV , and the relative spatial variation of the coordination number, $\delta z/z$ versus $\phi - \phi_c$, respectively, with the lines guide to eye.

particle potential independent exponents. The new scalings from the best fits to our data are

$$V \sim \phi - \phi_c, \quad B \sim \phi^2, \quad G \sim \phi, \quad z \sim \phi - \phi_c. \quad (2)$$

The pressure $p \sim \phi^2$ can be derived from the relation $p = \frac{\phi}{L^3} \frac{dV}{d\phi}$, where L is the length of the simulation box. The moduli scale with ϕ instead of $\phi - \phi_c$ because they are derivatives of the stresses which scale with ϕ as the pressure does. Apparently, ϕ_d divides jamming into two distinct regimes: marginal jamming with interaction dependent material properties and deep jamming insensitive to the inter-particle potential.

At fixed pressure, the distribution of the potential energy of distinct jammed states is Gaussian. The half height width of the Gaussian distribution, δV is plotted versus $\phi - \phi_c$ in the inset to Fig. 1(a). Interestingly,

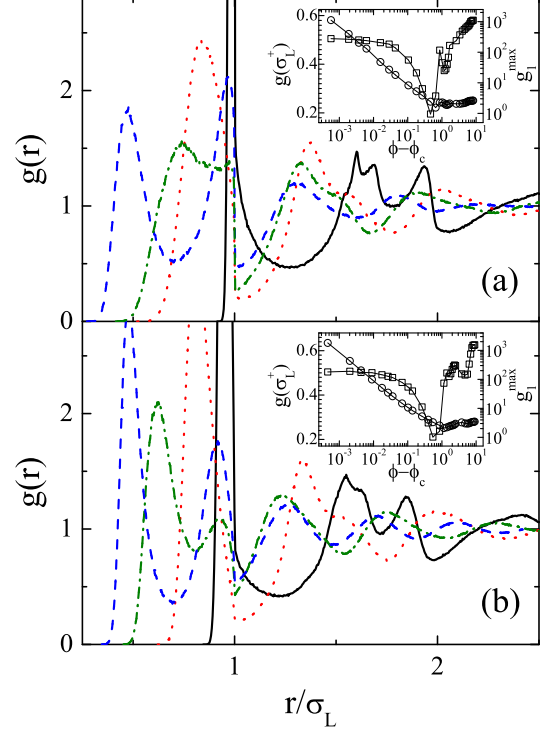


FIG. 2: (color online) Pair distribution function of large particles, $g(r)$ for (a) harmonic and (b) Hertzian systems. The black solid, red dotted, green dot-dashed, and blue dashed lines are at $\phi - \phi_c \approx 0.044, 0.46, 0.66$, and 1.68 in (a) and $0.14, 0.54, 1.14$, and 2.50 in (b). The insets show $g(r)$ at $r = \sigma_L^+$, $g(\sigma_L^+)$ (squares) and the first peak, g_1^{\max} (circles) versus $\phi - \phi_c$, with the lines guide to eye.

δV behaves different volume fraction dependence on both sides of ϕ_d : $\delta V \sim (\phi - \phi_c)^\alpha$ when $\phi < \phi_d$, and roughly a constant otherwise.

In marginally jammed solids, spatial fluctuations are significant, e.g. the distribution of local coordination number is broad [14, 26]. In the inset to Fig. 1(c) we plot the relative spatial fluctuation of the coordination number, $\delta z/z$ versus the volume fraction. When $\phi < \phi_d$, $\delta z/z$ decreases with increasing ϕ and drops to the minimum at ϕ_d , so the spatial fluctuations in marginally jammed solids indeed decrease with increasing ϕ . When $\phi > \phi_d$, however, $\delta z/z$ increases with ϕ , leading to the growth of spatial fluctuations. Fluctuations in deeply jammed solids are thus not to be neglected, contrary to the expectation of more homogeneous and “mean field” solids at high volume fractions.

Marginally jammed solids undergo some structural changes in the pair distribution function $g(r)$ during the jamming transition [14–16]. The first peak of $g(r)$, g_1^{\max} behaves a power law divergence approaching Point J. Meanwhile, the second peak splits into subpeaks at $r = \sqrt{3}$ and 2 in unit of particle diameter, which become discontinuous at Point J. Another anomalous feature is the discontinuity at $r = 1$ above Point J, implying that

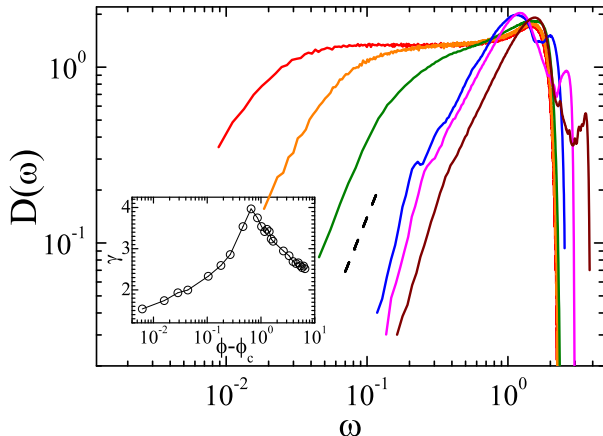


FIG. 3: (color online) Density of states, $D(\omega)$ of jammed solids with harmonic interactions. From the left to the right, the solid curves are measured at $\phi - \phi_c \approx 0.0006$ (red), 0.0062 (orange), 0.044 (green), 0.46 (blue), 1.68 (magenta), and 4.48 (maroon). The dashed line shows the Debye behavior with a slope of 2. The inset shows the exponent γ of the power law fit, $D(\omega) \sim \omega^\gamma$ to the low frequency part of $D(\omega)$ versus $\phi - \phi_c$, with the line guide to eye.

pairs of particles that are just in contact with each other are more than those that are almost in touch [14].

There are also structural signatures in $g(r)$ associated with the crossover at ϕ_d , as shown in Fig. 2 of $g(r)$ of large particles. When $\phi < \phi_d$, there is only one peak in $g(r)$ at $r < \sigma_L$, where σ_L is the large particle diameter. At ϕ_d , a second peak starts to emerge on the left-hand side of $r = \sigma_L$, which locates at almost the same r in unit of σ_L when the volume fraction increases. Moreover, the insets to Fig. 2 show that both the first peak, g_1^{\max} and the right-hand side of $r = \sigma_L$, $g(\sigma_L^+)$ reach their minima at ϕ_d . These three robust changes in $g(r)$ structurally distinguish deeply and marginally jammed solids.

A special feature of marginally jammed solids is the presence of a plateau in the density of vibrational states $D(\omega)$ [7]. The plateau extends to $\omega = 0$ at Point J, implying the existence of excess soft modes at the jamming transition. It has been argued that $D(\omega)$ deviates from the Debye law ($D(\omega) \sim \omega^{d-1}$) especially close to Point J [7]. However, for finite size systems, low-frequency modes are sparse and discrete in frequency, leading to difficulties in determining the exact behavior of the low-frequency $D(\omega)$. Furthermore, due to finite size effects, plane-waves hybridize with anomalous modes at low frequencies [8, 13]. It is still a mystery if plane-wave-like modes could eventually dehybridize with anomalous modes and recover the Debye-like $D(\omega)$ at the low-frequency end in the thermodynamic limit.

We diagonalize the Hessian matrix using ARPACK [27] to obtain the normal modes of vibration. Figure 3 shows the density of states $D(\omega)$ for both marginally and deeply jammed solids with harmonic interactions [28]. $D(\omega)$ at

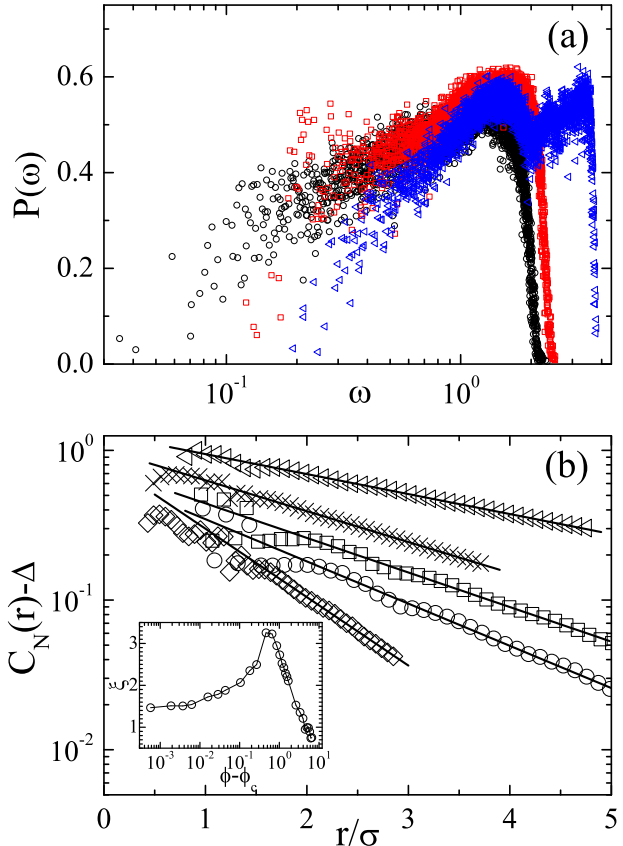


FIG. 4: (color online) (a) Participation ratio, $P(\omega)$ of jammed solids with harmonic interactions at $\phi - \phi_c \approx 0.044$ (black circles), 0.46 (red squares), and 4.48 (blue triangles). (b) Normalized correlation of the polarization vectors, $C_N(r)$ of the lowest frequency mode at $\phi - \phi_c \approx 0.0062$ (circles), 0.044 (squares), 0.46 (left triangles), 1.68 (crosses), and 4.48 (diamonds). The solid lines are fits according to $C_N(r) = C_0 \exp(-r/\xi) + \Delta$. The inset to (b) shows ξ versus $\phi - \phi_c$, with the line guide to eye.

the low frequency end can be approximately fitted with $D(\omega) \sim \omega^\gamma$. The inset to Fig. 3 does not support the Debye picture, i.e. $\gamma = 2$. Our data indicate that $\gamma < 2$ close to the jamming transition at Point J. It increases with increasing ϕ , but does not stop at $\gamma = 2$. Interestingly, γ reaches its maximum (~ 4) at the crossover volume fraction ϕ_d . In deeply jammed solids, γ decreases with increasing ϕ . Debye behavior is completely absent in deeply jammed solids studied here, which is another strong evidence supporting that deeply jammed solids are quite different from normal solids.

The anomalous density of states comes along with quasi-localization at low frequencies. Figure 4(a) shows the participation ratio of normal modes, defined as $P(\omega) = \frac{(\sum |\vec{e}_i^\omega|^2)^2}{N \sum |\vec{e}_i^\omega|^4}$, where \vec{e}_i^ω is the polarization vector of particle i in the mode at ω , and the sums are over all

particles. In both marginally and deeply jammed solids, there are always quasi-localized modes with low $P(\omega)$ at low frequencies. In marginally jammed solids, the quasi-localization is weaker with increasing ϕ , expressed in the decrease of the number of quasi-localized modes and the increase of the minimum $P(\omega)$. Figure 4(a) shows that at ϕ_d there are quite a few low-frequency modes with large participation ratio forming a bump in $P(\omega)$, indicating the increase of the plane-wave components. When $\phi > \phi_d$, however, quasi-localization is strengthened with increasing ϕ .

To quantify how the quasi-localization varies with the volume fraction, we measure the correlation of polarization vectors in the lowest frequency mode: $C(r) = \langle \vec{e}_i^{\omega_{\min}} \cdot \vec{e}_j^{\omega_{\min}} \rangle$, where $\langle \dots \rangle$ denotes the average over configurations and all pairs of particles i and j with a separation of r . Figure 4(b) shows that the normalized correlation $C_N(r) = C(r)/C(0)$ can be well fitted with $C_N(r) = C_0 \exp(-r/\xi) + \Delta$, where $C_0 > 0$ and $\Delta < 0$. The parameter ξ characterizes the size of the quasi-localized regions. The inset to Fig. 4(b) shows that ξ is less than four particle sizes and reaches its maximum at the crossover volume fraction ϕ_d , so the lowest frequency mode at ϕ_d is the least localized.

All the results shown in this letter suggest that deeply jammed solids at $\phi > \phi_d$ are new amorphous materials other than normal solids or marginally jammed solids. It is intriguing that most properties of jammed systems undergo remarkable changes at the same crossover volume fraction. The special features of deeply jammed solids must have significant impact on dynamics of thermal and sheared systems at very high volume fractions. We observe that the glass transition temperature increases with the volume fraction up to ϕ_d and drops afterwards [29], in consistent with a recent observation that increasing the density lowers the glass transition of ultrasoft colloids [30]. We would expect similar volume fraction dependence of the yield stress. Based on this picture, the jamming phase diagram [1, 16] may need corrections at high volume fractions for systems with soft potentials. Deeply jammed solids are accessible in experiments of core-softened colloids interacting via long-range electrostatic repulsions [31]. We hope that the present work could open a route to explore this new kind of amorphous materials.

This work was supported by the National Natural Science Foundation of China (No. 91027001) and startup grant from USTC.

* ningxu@ustc.edu.cn

- [1] A. J. Liu and S. R. Nagel, *Nature (London)* **396**, 21 (1998).
- [2] A. J. Liu and S. R. Nagel, *Ann. Rev. of Cond. Mat. Phys.* **1**, 347 (2010).
- [3] M. van Hecke, *J. Phys: Condens. Matter* **22**, 033101 (2010).
- [4] N. Xu, *Front. of Phys. in China*, doi:10.1007/s11467-010-0102-y (2010).
- [5] C. S. O'Hern, S. A. Langer, A. J. Liu, and S. R. Nagel, *Phys. Rev. Lett.* **88**, 075507 (2002); C. S. O'Hern, L. E. Silbert, A. J. Liu, and S. R. Nagel, *Phys. Rev. E* **68**, 011306 (2003).
- [6] P. Olsson and S. Teitel, *Phys. Rev. Lett.* **99**, 178001 (2007).
- [7] L. E. Silbert, A. J. Liu, and S. R. Nagel, *Phys. Rev. Lett.* **95**, 098301 (2005).
- [8] M. Wyart, S. R. Nagel, and T. A. Witten, *Europhys. Lett.* **72**, 486 (2005); M. Wyart, L. E. Silbert, S. R. Nagel, and T. A. Witten, *Phys. Rev. E* **72**, 051306 (2005).
- [9] J. A. Drocco, M. B. Hastings, C. J. O. Reichhardt, and C. Reichhardt, *Phys. Rev. Lett.* **95**, 088001 (2005).
- [10] W. G. Ellenbroek, E. Somfai, M. van Hecke, and W. van Saarloos, *Phys. Rev. Lett.* **97**, 258001 (2006).
- [11] A. S. Keys, A. R. Abate, S. C. Glotzer, and D. J. Durian, *Nat. Phys.* **3**, 260 (2007).
- [12] D. A. Head, *Phys. Rev. Lett.* **102**, 138001 (2009).
- [13] N. Xu, V. Vitelli, M. Wyart, A. J. Liu, and S. R. Nagel, *Phys. Rev. Lett.* **102**, 038001 (2009); V. Vitelli, N. Xu, M. Wyart, A. J. Liu, and S. R. Nagel, *Phys. Rev. E* **81**, 021301 (2010).
- [14] L. E. Silbert, A. J. Liu, and S. R. Nagel, *Phys. Rev. E* **73**, 041304 (2006).
- [15] A. Donev, S. Torquato, and F. H. Stillinger, *Phys. Rev. E* **71**, 011105 (2005).
- [16] Z. Zhang, N. Xu, D. T. N. Chen, P. Yunker, A. M. Alsayed, K. B. Aptowicz, P. Habdas, A. J. Liu, S. R. Nagel, and A. G. Yodh, *Nature (London)* **459**, 230 (2009).
- [17] D. J. Durian, *Phys. Rev. Lett.* **75**, 4780 (1995).
- [18] L. E. Silbert, A. J. Liu, and S. R. Nagel, *Phys. Rev. E* **79**, 021308 (2009).
- [19] N. Xu, V. Vitelli, A. J. Liu, and S. R. Nagel, *Europhys. Lett.* **90**, 56001 (2010).
- [20] K. Chen *et al.*, *Phys. Rev. Lett.* **105**, 025501 (2010).
- [21] A. Ghosh, V. K. Chikkadi, P. Schall, J. Kurchan, and D. Bonn, *Phys. Rev. Lett.* **104**, 248305 (2010).
- [22] C. Brito, O. Dauchot, G. Biroli, and J. P. Bouchaud, *Soft Matter* **6**, 3013 (2010).
- [23] D. Kaya, N. L. Green, C. E. Maloney, and M. F. Islam, *Science* **329**, 656 (2010).
- [24] <http://www.ece.northwestern.edu/~nocedal/lbfgs.html>.
- [25] All the results reported in this letter are valid for systems with $\alpha = 3$ as well, which are not shown here.
- [26] N. Xu and E. S. C. Ching, *Soft Matter* **6**, 2944 (2010).
- [27] <http://www.caam.rice.edu/software/ARPACK>.
- [28] For Hertzian systems not shown here, we observe similar volume fraction dependence of both the density of states and participation ratio.
- [29] L. J. Wang and N. Xu, unpublished (2010).
- [30] L. Berthier, A. J. Moreno, and G. Szamel, *Phys. Rev. E* **82**, 060501(R) (2010).
- [31] N. Osterman, D. Babic, I. Poberaj, J. Dobnikar, and P. Ziherl, *Phys. Rev. Lett.* **99**, 248301 (2007).